DENTAL MATERIALS 35 (2019) 970–978

Available online at www.sciencedirect.com

ScienceDirect

journal homepage: www.intl.elsevierhealth.com/journals/dema

Improvement of mechanical properties of Y-TZP by thermal annealing with monoclinic zirconia nanoparticle coating

Masahiro Okada[a], *Hiroaki Taketa*[b], *Emilio Satoshi Hara*[a], *Yasuhiro Torii*[b], *Masao Irie*[a], *Takuya Matsumoto*[a,*]

[a] *Department of Biomaterials, Graduate School of Medicine, Dentistry and Pharmaceutical Sciences, Okayama University, 2-5-1 Shikata-cho, Kita-ku, Okayama 700-8558, Japan*

[b] *Department of Comprehensive Dentistry, Okayama University Hospital, 2-5-1 Shikata-cho, Kita-ku, Okayama 700-8558, Japan*

ARTICLE INFO

Article history:
Received 13 November 2018
Received in revised form
27 February 2019
Accepted 1 April 2019

Keywords:
Yttria-stabilized tetragonal zirconia polycrystals
Monoclinic phase
Biaxial flexural strength
Thermal annealing

ABSTRACT

Objective. To assess whether a thermal annealing with a monoclinic zirconia (mZrO$_2$) nanoparticle coating can improve the reliability of sandblasted yttria-stabilized tetragonal zirconia polycrystals (Y-TZP) and maintain its mechanical strength.

Methods. Commercially available Y-TZP (Lava Frame, 3M Dental Products) disks were sintered and surface-treated as follows: AS (as sintered, with no treatment); SB (sandblasting); SB-TA (sandblasting followed by thermal annealing at 1000 °C); and SB-mZr-TA (sandblasting followed by thermal annealing at 1000 °C with the mZrO$_2$ nanoparticle coating). The mZrO$_2$ nanoparticles of 21 nm in size were prepared by a hydrothermal method, and coated onto Y-TZP sintered disks as a 5 g/L ethanol dispersion. Biaxial flexural strength (S) was measured using the piston-on-three-ball test, and reliability was evaluated by the Weibull modulus (m).

Results. Biaxial flexural tests showed a significant increase in the strength of Group SB ($S_{SB} = 1445 \pm 191$ MPa) compared with Group AS ($S_{AS} = 1071 \pm 112$ MPa). The thermal annealing improved the reliabilities of the sandblasted Y-TZP ($m_{SB\text{-}TA} = 20.14$ and $m_{SB\text{-}mZr\text{-}TA} = 21.33$), as compared with Group SB ($m_{SB} = 7.77$). However, the conventional thermal annealing without the mZrO$_2$ coating caused a significant decrease in the strength of sandblasted Y-TZP ($S_{SB\text{-}TA} = 1273 \pm 65$ MPa). Importantly, the mZrO$_2$ coating prevented the decrease in the strength caused by conventional thermal annealing ($S_{SB\text{-}mZr\text{-}TA} = 1379 \pm 65$ MPa).

Significance. The thermal annealing with the mZrO$_2$ nanoparticle coating can improve the reliability of sandblasted Y-TZP and maintain its mechanical strength, which would otherwise be decreased by the conventional annealing process.

1. Introduction

In recent years, all-ceramic restorations have been increasingly used for medium-to-large tooth reconstructions [1].

* *Corresponding author.*
E-mail address: tmatsu@md.okayama-u.ac.jp (T. Matsumoto).

https://doi.org/10.1016/j.dental.2019.04.002

Owing to their superior mechanical properties, zirconia-based ceramics, especially yttria-stabilized tetragonal zirconia polycrystals (Y-TZP), can be used as alternative to conventional metal frameworks [2–4]. Transformation toughening along with microcracking and deflection mechanisms are the toughening mechanisms now prominent in zirconia-based ceramics [5].

The major clinical problem with the use of zirconia-based ceramics is the difficulty in achieving suitable bonding to luting agents [6–8] or veneering ceramics [9,10]. Airborne-particle abrasion (mainly sandblasting with alumina particles) is commonly used to improve bonding, as this procedure cleans the ceramic surface, removes impurities, increases surface roughness, and modifies the surface energy and wettability [11,12].

The airborne-particle abrasion applied to Y-TZP surfaces can also induce protective compressive residual stress on their surfaces *via* tetragonal to monoclinic phase transformation [12], thereby initially increasing flexural strength. However, previous studies have indicated a decreased reliability of Y-TZP after mechanical surface treatments, depending on the degree of induced surface damage [13–15]. Considering that mechanical surface treatments can exert both positive and negative effects on Y-TZP, some researchers and manufacturers recommend thermal annealing as a "regeneration firing" for the re-establishment of the tetragonal phase and to increase the reliability of Y-TZP, even though it causes a decrease in flexural strength [16,17]. The correlation between the flexural strength and monoclinic phase content of Y-TZP upon mechanical and annealing treatments was first reported by Kosmac et al. [13] They showed that thermal annealing caused a reverse transformation (*i.e.*, the monoclinic phase content of sandblasted Y-TZP decreased to a plateau value after annealing above 900 °C) that released the compressive stress and decreased flexural strength.

In this study, we propose a novel method to improve the reliability of sandblasted Y-TZP without decreasing its mechanical strength by a thermal annealing with a non-stabilized (*i.e.*, yttrium-free) monoclinic zirconia ($m$$ZrO_2$) nanoparticle coating. This idea was generated based on the assumption that the yttrium-free $m$$ZrO_2$ coating on a sandblasted Y-TZP substrate could induce protective compressive residual stress after thermal annealing due to mismatching of the thermal expansion coefficients of monoclinic coating layer ($m$$ZrO_2$) [18] and tetragonal substrate (Y-TZP) [19]. The null hypothesis was that there is no difference in both the biaxial flexural strength and the Weibull modulus of Y-TZP after sandblasting followed by thermal annealing with $m$$ZrO_2$ nanoparticles, as compared with only sandblasting or conventional thermal annealing.

2. Materials and methods

2.1. Materials

Reagent-grade $ZrOCl_2 \cdot 8H_2O$, poly(acrylic acid) (PAA; molecular weight, 5000) used as a binder, and ethanol were used as-received from Wako Pure Chemical Industries, Ltd. (Osaka, Japan). Pre-sintered 3 mol% Y-TZP (Lava Frame Zirconia) was kindly donated by 3M ESPE Dental Products (Seefeld, Germany). Milli-Q water (Millipore Corp., Bedford, MA) with a specific resistance of $18.2 \times 10^6\ \Omega$ cm was used for all solutions.

2.2. $mZrO_2$ nanoparticles

First, $m$$ZrO_2$ nanoparticles were prepared *via* the hydrothermal method using 4 mol/L $ZrOCl_2 \cdot 8H_2O$ aqueous solution in an oil bath at 200 °C for 100 h [20,21]. The resultant white precipitate was centrifugally washed with water and re-dispersed in ethanol.

For scanning electron microscope (SEM) observation, the dispersed sample was dried on an aluminum stub and osmium coating was conducted using a Neoc-Pro osmium coater (Meiwafosis Co., Ltd., Tokyo, Japan). The particle morphology was observed using a JSM-6701F scanning electron microscope (JEOL Ltd., Tokyo, Japan) operating at 5 kV. The number-averaged particle size ($N = 50$) was determined from the SEM photographs using image analysis software (Image J; National Institutes of Health, Bethesda, MD, USA). Product identification was achieved by using X-ray diffraction (XRD) measurements (RINT2500HF; Rigaku Corp., Tokyo, Japan) with Cu-Kα (1.54 Å) irradiation at 40 kV and 200 mA from 5 to 60° at a scan speed of 2°/min.

The $m$$ZrO_2$ dispersion was mixed with an equal volume of 1 wt% PAA ethanol solution and the final concentration of $m$$ZrO_2$ was 5 g/L.

2.3. Y-TZP samples

A low-speed cutting machine was used to cut the pre-sintered Y-TZP into pieces of approximately 18 mm in diameter and 1.4 mm in thickness under tap water irrigation. After the disks were sintered at 1500 °C for 2 h (heating rate: 20 °C/min from room temperature (around 20 °C) to 800 °C; 10 °C/min from 800 to 1500 °C; cooling rate: <15 °C/min), the Y-TZP ceramics (approximately 14 mm in diameter and 1.2 mm in thickness) were randomly submitted to the following treatments.

2.3.1. As-sintered (AS)

The samples after sintering were used without further treatment.

2.3.2. Sandblasting (SB)

After sintering, both sides of the disks were ground sequentially with #120, #320, and #600 silicon carbide abrasive papers (Buehler, Illinois Tool Works Inc., IL, USA) to obtain a flat uniform surface under tap water irrigation to remove contaminants. Each abrasive paper was exchanged and a new paper was used after grinding one side of each disk. After grinding, one side of each disk was then sandblasted with 50 μm alumina particles using a laboratory sandblaster (Hi-Blaster III, Shofu Inc., Kyoto, Japan) at 0.25 MPa for 10 s at a distance of 10 mm [22]. After sandblasting, each disk was separately cleaned with pure water three times, replacing the water each time in an ultrasonic cleaner (ASU-2D; AS ONE Corp., Osaka, Japan) set at 23 kHz for 1 min.

2.3.3. *Sandblasting followed by thermal annealing (SB-TA)*

The sandblasted samples were thermally treated at 1000 °C for 1 min (heating rate: 10 °C/min; cooling rate: <10 °C/min).

2.3.4. *Sandblasting followed by thermal annealing with $mZrO_2$ nanoparticle coating (SB-mZr-TA)*

The sandblasted samples were applied with a $mZrO_2$ dispersion (0.2 μL/mm²–sample surface area; *i.e.*, 30 μL in the case of the sample disk with 14 mm in diameter) using a micropipette, and left to dry at room temperature for around 10 min. The samples were then thermally treated at 1000 °C for 1 min (heating rate: 10 °C/min; cooling rate: <10 °C/min).

2.4. *Biaxial flexural tests*

The biaxial flexural tests ($N = 15$) were performed using the piston-on-three ball technique [23] in a universal testing machine (Autograph AG-X, Shimadzu Corp., Kyoto, Japan). Three 3.2 mm diameter stainless-steel balls were placed on a circle with a diameter of 10 mm equidistant from each other. The disks were placed centrally and faced the steel balls, and a load was applied with a 1.2 mm diameter piston at a crosshead speed of 1.0 mm/min. The fracture load for each specimen was recorded and the biaxial flexural strength was calculated using Eq. (1):

$$S = \frac{-0.2387\,P\,(X-Y)}{d^2} \tag{1}$$

where S is biaxial flexural strength (MPa); P is fracture load (N); and d is specimen disk thickness at the fracture origin (mm). The X and Y parameters were determined as follows:

$$X = (1+\upsilon)\ln\left(\frac{r_2}{r_3}\right)^2 + \left[\frac{1-\upsilon}{2}\right]\left(\frac{r_2}{r_3}\right)^2 \tag{2}$$

$$Y = (1+\upsilon)\left[1+\ln\left(\frac{r_1}{r_3}\right)^2\right] + (1-\upsilon)\left(\frac{r_1}{r_3}\right)^2 \tag{3}$$

where υ is Poisson's ratio (0.25), r_1 is the radius of the support circle, r_2 is the radius of the loaded area, and r_3 is the radius of the sample.

The Steel-Dwass test was performed using R version 3.3.2 [24] at preset alpha levels of 0.05 to detect multiple comparisons among the four experimental groups. The Weibull analysis of the data was also performed to determine the Weibull moduli [25]. The goodness-of-fit for Weibull distribution was evaluated from the coefficient of determination (R^2) [26]. The increase in the Weibull moduli of Groups SB-TA or SB-*m*Zr-TA, as compared with that of Group SB, was statistically evaluated according to the method developed by Hudak and Tiryakioğlu [27] and the preset alpha levels were set to 0.05/2 (=0.025) in order to keep the familywise error rate of 0.05 after the multiple comparisons (two times).

2.5. *Surface characterizations*

Phase transformations induced by the applied surface treatments were determined by analysis of the XRD patterns of the samples. The XRD patterns were collected with a $\theta/2\theta$ diffractometer (RINT2500HF) using Cu-Kα (1.54 Å) irradiation at 40 kV and 200 mA. The XRD patterns were obtained from 27 to 37° at a scan speed of 1°/min. The monoclinic peak intensity ratio (X_m) was calculated using the method reported by Garvie and Nicholsone [28] as follows:

$$X_m = \frac{I_m\left(\bar{1}11\right) + I_m\left(111\right)}{I_m\left(\bar{1}11\right) + I_m\left(111\right) + I_t\left(111\right)} \tag{4}$$

where I_t and I_m represent the integrated intensities of the tetragonal (111) peak and monoclinic (111) and (−111) peaks at approximately 30°, 31°, and 28.2°, respectively. Monoclinic phase content (F_m) was calculated using the method reported by Taraya et al. [29] as follows:

$$F_m = \frac{1.311\,X_m}{1+0.311\,X_m} \tag{5}$$

The total monoclinic phase thickness was obtained from transformed zone depth (TZD) calculated according to the following equation [30,31]:

$$TZD = \left[\frac{\sin\theta}{2\mu}\right]\left[\ln\left(\frac{1}{1-F_m}\right)\right] \tag{6}$$

where θ (15°) is the angle of reflection, and μ (0.0642) is the absorption coefficient. The thickness of monoclinic phase remained in Y-TZP substrate was estimated by subtracting the thickness of the $mZrO_2$ coating layer, which was calculated from the applied amount and density of $mZrO_2$, from the total monoclinic phase thickness determined by TZD.

The surfaces of the samples were observed by using a JSM-6701F scanning electron microscope operated at 5 kV after coating with a Neoc-Pro osmium coater.

The average surface roughness (Ra) of each sample was determined using a profilometer (HandySurf E-35B; Mitutoyo Corp., Kanagawa, Japan) with active tip radius of 2 μm, reading length of 2.0 mm, and reading speed of 0.6 mm/s. Three measurements at different locations were recorded for each specimen, and the values were averaged.

Vickers hardness (HV) was measured using a microhardness tester (FM-700, Future-Tech Corp., Kanagawa, Japan) with 1000 gf for 15 sec. The measurements were performed on three separate points for each sample.

3. Results

3.1. *$mZrO_2$ nanoparticles*

The SEM photograph shows that the number-averaged particle size was 21 ± 5 nm (Fig. 1a). From the XRD pattern, the product was determined to be monoclinic zirconia and no other crystal phase was observed (Fig. 1b). The $mZrO_2$ nanoparticles after centrifugal washing were dispersed in ethanol (5 g/L) containing 1 wt% PAA as a binder. Ethanol was used as a dispersion medium to promote fast drying and allow a uniform surface coating. The thermal treatment (up to 1000 °C) of the $mZrO_2$ nanoparticles did not change their crystal phase, but each peak in the XRD pattern sharpened as the thermal treatment

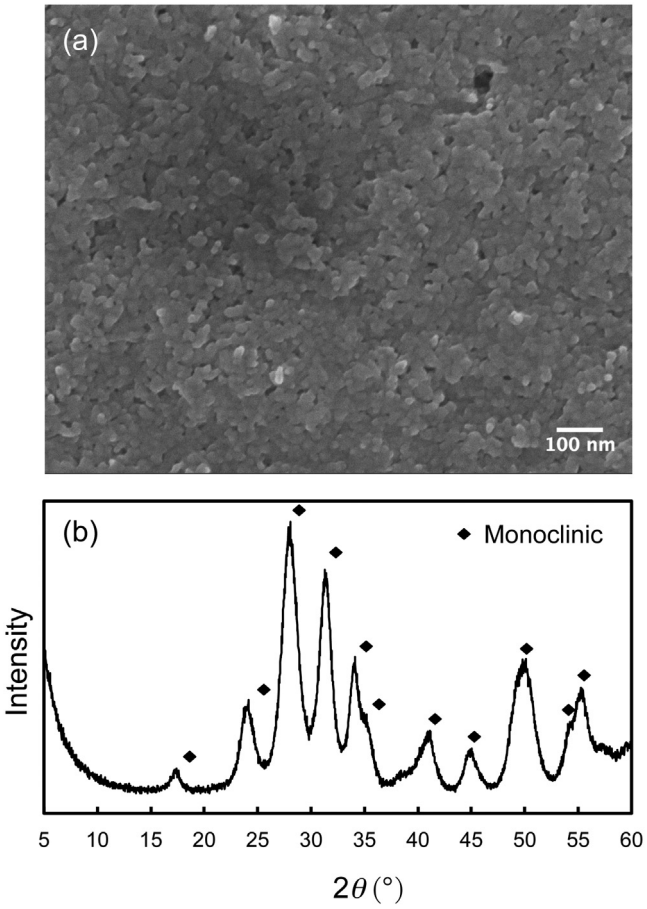

Fig. 1 – (a) SEM photograph and (b) XRD pattern of the $mZrO_2$ nanoparticles prepared by hydrothermal treatment at 200 °C.

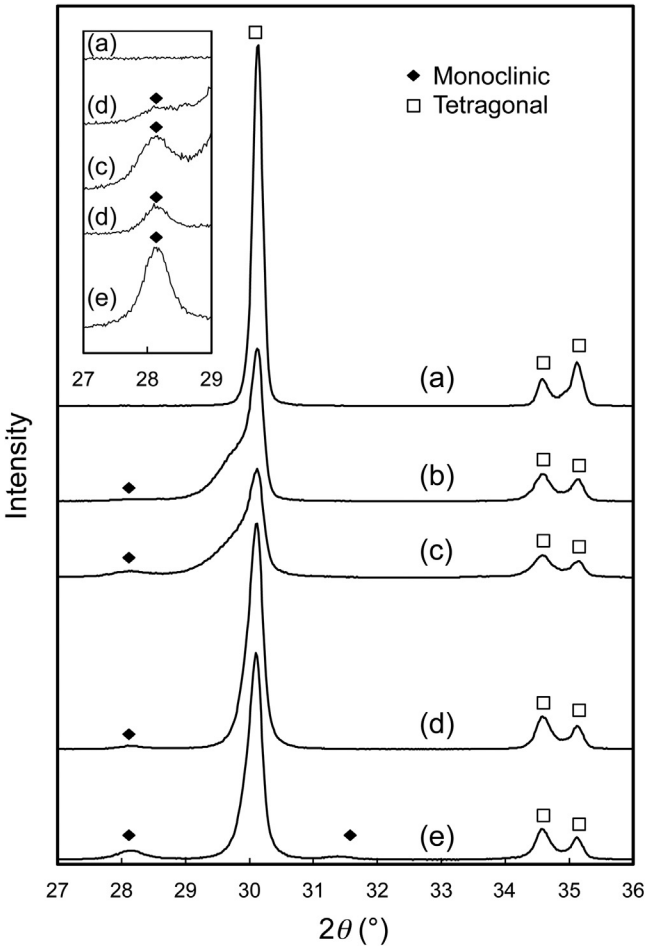

Fig. 2 – XRD patterns of (a: Group AS) as-sintered, (b) wet ground, (c: Group SB) sandblasted, and annealed Y-TZP (d: Group SB-TA) without and (e: Group SB-mZr-TA) with $mZrO_2$ coating. The annealing was performed at 1000 °C. $mZrO_2$ coating was performed at 0.2 μL/mm^2. The inset shows the magnified region.

temperature was increased (Supplemental Fig. S1), indicating successful sintering and crystal growth.

3.2. *XRD measurements*

Fig. 2a shows the XRD pattern of the AS samples, showing only a tetragonal phase. After grinding, the tetragonal (111) peak at a 2θ of 30.2° was broadened and the full width at half maximum (FWHM) of the peak increased from 0.177 to 0.339 (Fig. 2b). In Fig. 2b, the monoclinic (−111) peak at a 2θ of 28.2° was detected, and the monoclinic phase content was determined to be 1.9% after grinding. The monoclinic content and FWHM increased to 9.7% and 0.436, respectively, after sandblasting (Fig. 2c). After annealing at 1000 °C without $mZrO_2$ coating, the monoclinic phase peaks decreased to 2.8%, and the tetragonal (111) peak became sharper (FWHM, 0.259), as shown in Fig. 2d. The monoclinic phase peaks were clearly observed after annealing with $mZrO_2$ coating (Fig. 2e) while the tetragonal (111) peak became sharper (FWHM, 0.249) compared with that observed before annealing.

The monoclinic phase content and total monoclinic phase thickness of the $mZrO_2$-coated sample after annealing increased approximately linearly by increasing the amount of $mZrO_2$ coating (Fig. 3 and Supplemental Fig. S2 with closed circles). However, these values decreased after ultrasonic washing of the samples coated above 0.3 μL/mm^2 (Fig. 3a and Supplemental Fig. S2 with open triangles), suggesting a coating layer breakage when a thick coating was applied. The thickness of monoclinic phase remained in the Y-TZP substrate, which was estimated by subtracting the $mZrO_2$ coating thickness (calculated from the coating amount and density of $mZrO_2$) from the total monoclinic phase thickness determined by TZD, increased over the coating range of 0–0.2 μL/mm^2 and plateaued above 0.2 μL/mm^2 (Fig. 3b). These results suggest a strong interaction between the $mZrO_2$ coating layer and the Y-TZP substrate, and that the coating layer near substrate surface prevented the monoclinic-to-tetragonal reverse transformation of the Y-TZP substrate surface by thermal annealing.

3.3. *Surface characterizations*

The Ra (Fig. 4) and HV (Supplemental Fig. S3) were measured using Y-TZP coated with different amounts of $mZrO_2$ followed

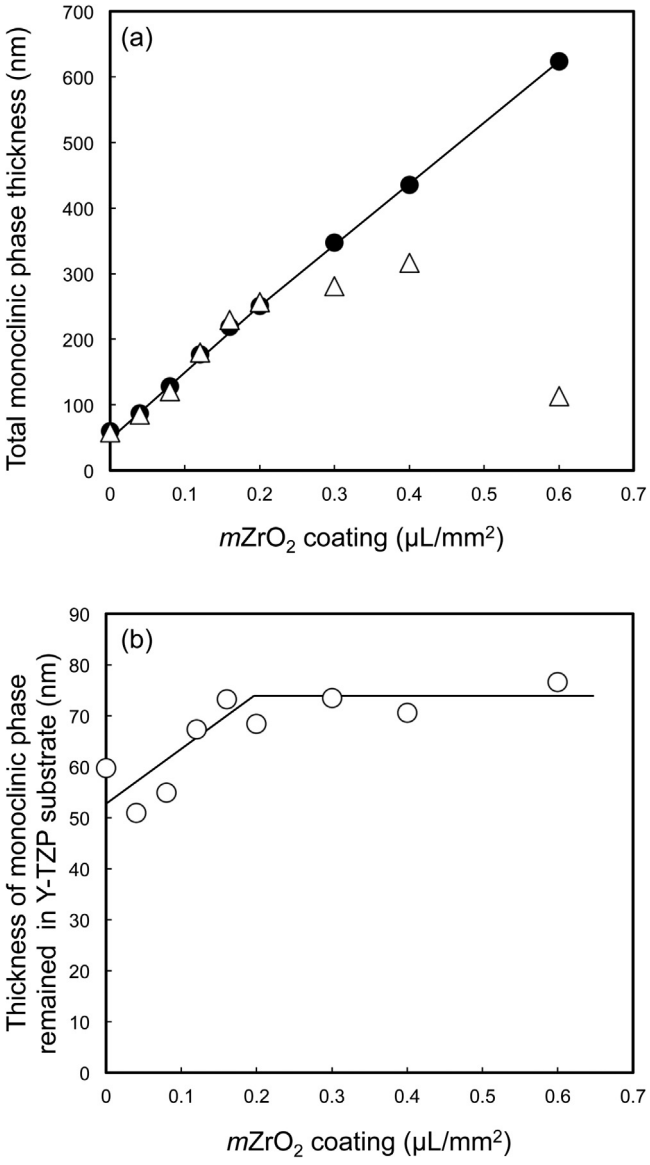

Fig. 3 – Variations in the total monoclinic phase thickness of $mZrO_2$-coated and thermally-annealed Y-TZP (a, closed circles) before and (a, open triangles) after ultrasonic washing treatments, and (b) the thickness of monoclinic phase remained in the Y-TZP substrate as a function of $mZrO_2$ coating. The thickness of monoclinic phase in the substrates was estimated by subtracting the $mZrO_2$ coating thickness, which was calculated from the coating amount and density of $mZrO_2$ (5.83 g/cm^3), from the total monoclinic phase thickness calculated from transformed zone depth (TZD) of the samples before ultrasonic washing.

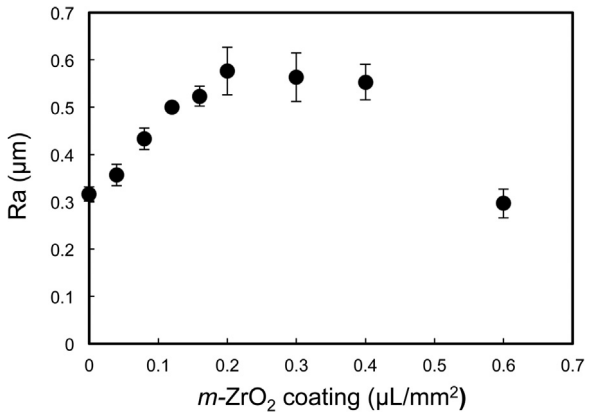

Fig. 4 – Surface roughness (Ra) values of the $mZrO_2$-coated Y-TZP after annealing followed by ultrasonic washing. The error bars represent the standard deviations (SD, N = 3).

by annealing and ultrasonic cleaning. The Ra values increased over the coating range of 0–0.2 μL/mm^2 and plateaued in the range of 0.2–0.4 μL/mm^2. For the 0.6 μL/mm^2 coating, the Ra values significantly decreased to same level as the non-coated samples. The HV values were not largely changed by the $mZrO_2$ coating.

Fig. 5 shows SEM photographs of the surfaces of non-coated (Group SB-TA) and $mZrO_2$-coated Y-TZP after annealing (Group SB-*m*Zr-TA). Note that in the $mZrO_2$-coated samples, spherical particles with number-averaged size of 71 ± 18 nm were observed uniformly on the substrate surface, indicating the sintering of $mZrO_2$ coating layer after annealing.

3.4. *Biaxial flexural strengths*

Fig. 6a summarizes the biaxial flexural strengths of the Groups AS, SB, SB-TA and SB-*m*Zr-TA. Sandblasting (Group SB) significantly increased the flexural strength of only-sintered Y-TZP (Group AS), but further thermal annealing without $mZrO_2$ coating (Group SB-TA) significantly decreased the strength. Importantly, the strength of the Group SB-*m*Zr-TA was not significantly different from that of Group SB, indicating the $mZrO_2$ coating could prevent the strength decrease induced by thermal annealing. Of note, the strength of Group SB-*m*Zr-TA was significantly higher than that of Group SB-TA.

The Weibull modulus (m) was determined from the Weibull plot (Fig. 6b) and used to assess the strength reliability, where larger values indicated greater strength reliability. Each R^2 value for Weibull fitting was larger than the critical points of R^2 at $\alpha = 0.05$ ($R^2_{0.05} = 0.878$ at $N = 15$ [26]), indicating that each Weibull fit was acceptable. The m_{AS}, m_{SB}, $m_{SB\text{-}TA}$ and $m_{SB\text{-}mZr\text{-}TA}$ were 9.78, 7.77, 20.14 and 21.33, respectively. In order to statistically evaluate the improvement of reliability after thermal annealing, the Weibull modulus ratios, compared to the Group SB, were respectively calculated ($m_{SB\text{-}TA}/m_{SB} = 2.593$ and $m_{SB\text{-}mZr\text{-}TA}/m_{SB} = 2.745$). These ratios were respectively above 97.5% confidence level (*i.e.*, $m_x/m_y > 2.069$ at $N = 15$ [27]), indicating a statistically significant improvement in the reliability of Groups SB-TA and SB-*m*Zr-TA, compared with Group SB.

4. Discussion

In this study, the Group AS was used as a control group to evaluate the mechanical strength increment [12] by sandblasting (Group SB), which was also used as another control group to evaluate the mechanical strength decrement and the reliability increment [16,17] after thermal annealing (Groups SB-TA and SB-*m*Zr-TA). The null hypothesis could be rejected from

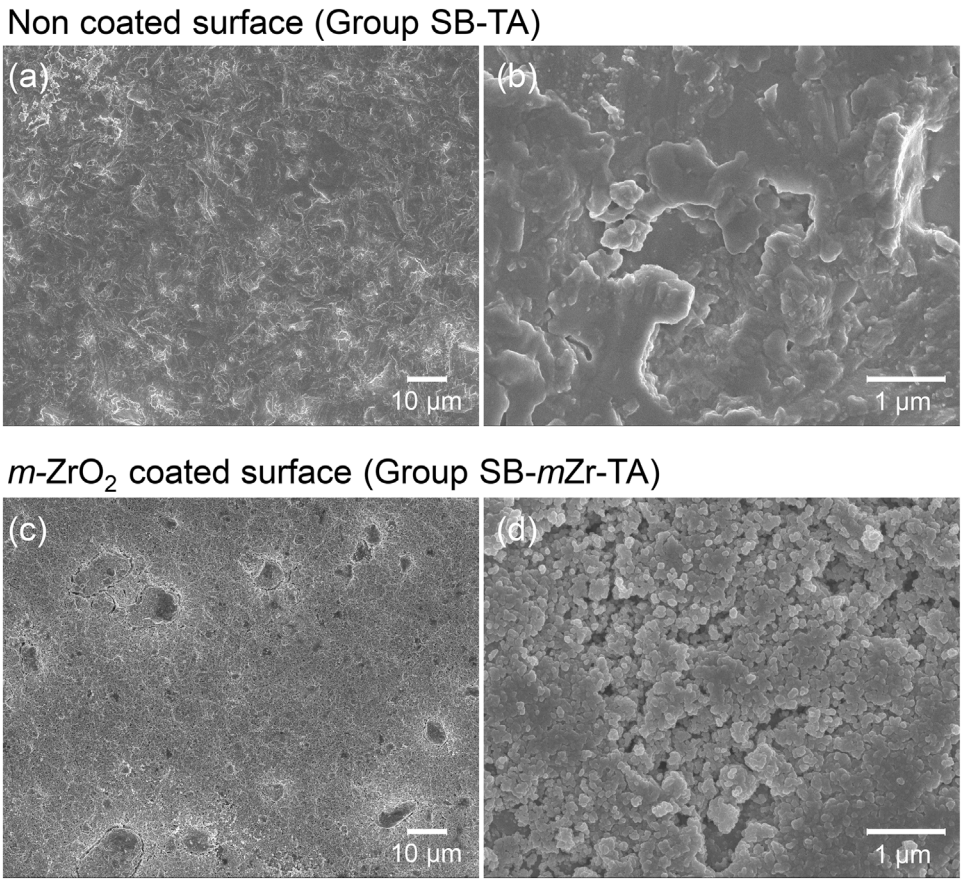

Fig. 5 – SEM photographs of the surfaces of (a, b: Group SB-TA) non-coated and (c, d: Group SB-*m*Zr-TA) $mZrO_2$-coated Y-TZP after annealing. The $mZrO_2$ coating was performed at 0.2 μL/mm^2.

the results shown of this study, and hence it was clear that the thermal annealing with the $mZrO_2$ nanoparticle coating could improve the reliability without decreasing the mechanical strength of sandblasted Y-TZP. Such improvement in the mechanical properties can facilitate the preparation of thinner zirconia-based dental prostheses and further improve their translucency.

One of the strengthening mechanisms behind the SB-$mZrO_2$-TA treatment should be the formation of compressive stress, which occurred during the cooling process after annealing due to the smaller thermal expansion coefficient of the $mZrO_2$ coating layer (approximately $6 \times 10^{-6}\,K^{-1}$ [18]) compared to that of the Y-TZP substrate (approximately $10 \times 10^{-6}\,K^{-1}$ [19]). Assuming that the $mZrO_2$ coating layer uniformly shrunk during the cooling process accompanied by the Y-TZP substrate shrinkage, the compressive strain in the coating layer was calculated to be 0.4%.

In this study, the crystal phase of the $mZrO_2$ coating layer should be unchanged during thermal annealing at 1000 °C. However, the compressive stress in the coating layer could be increased by inducing thermal crystal phase transformation at higher temperatures. The $mZrO_2$ (density, 5.83 g/cm^3) is thermodynamically stable at room temperature and undergoes transformation to tetragonal phase ($tZrO_2$; density, 6.1 g/cm^3) with volume change above 1077 °C [32]. The actual monoclinic-tetragonal phase transformation exhibits hysteresis, and the transformation temperature upon heating and cooling have been reported to be approximately 1227 and 927 °C, respectively [33,34]. Therefore, thermal annealing of the $mZrO_2$ coated samples above 1227 °C is expected to induce larger compressive stress by volume expansion upon cooling at approximately 927 °C, and is expected to improve mechanical properties to a more significant extent.

It should be noted that the non-doped (*i.e.*, yttrium-free) amorphous zirconia nanoparticles, which can be obtained by chemical precipitation or the sol-gel method, crystalizes into $tZrO_2$ at approximately 400 °C and the resultant $tZrO_2$ transforms into $mZrO_2$ above 600 °C [35,36]. The transformation of $tZrO_2$ into $mZrO_2$ is accompanied by volume expansion, which also induces surface compressive stress. Hence, non-doped amorphous zirconia nanoparticle coating is expected to be effective for improving the flexural strength of Y-TZP by annealing at lower temperatures. However, excessive compressive stress may induce crack formation in the coating layers.

In this study, nanoparticles were used for the $mZrO_2$ coating. Other coating methods, such as sol-gel coating, have the potential to improve the mechanical properties of Y-TZP. A recent study investigated a sol-gel coating zirconia, whose crystal phase was not reported, on a Y-TZP substrate [37], but the mechanical strength was unchanged after annealing at 550 °C. Previous data regarding the crystal phase transi-

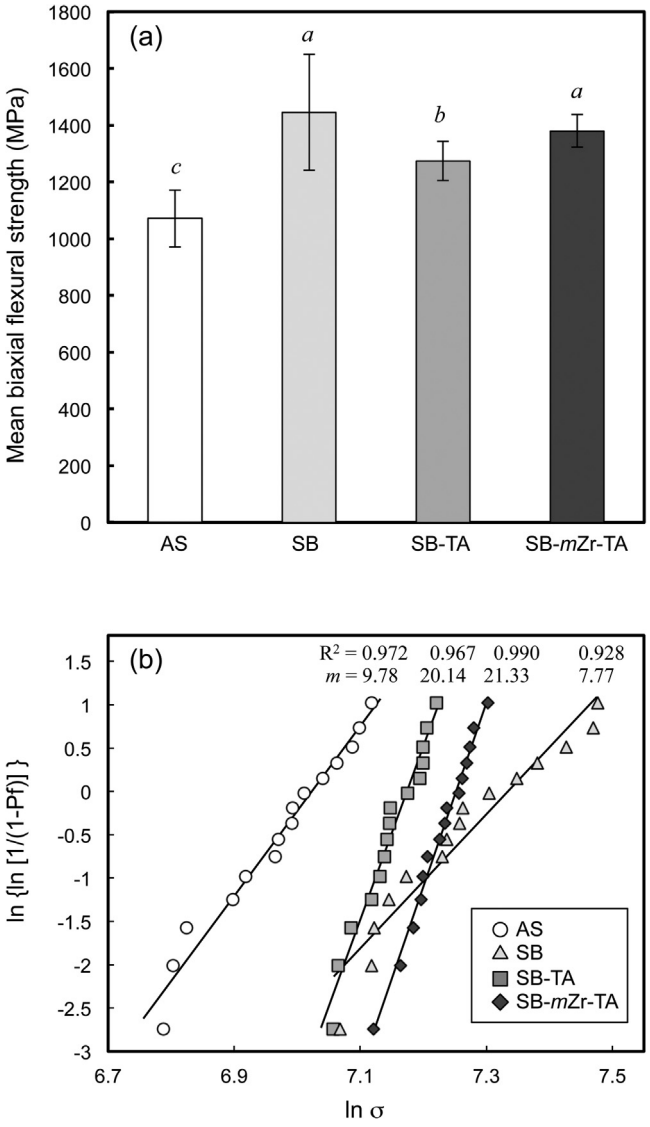

Fig. 6 – (a) Mean biaxial flexural strengths and (b) Weibull plots of Y-TZP. The error bars represent the standard deviations (SD, N = 15). Different italic letters (*a*, *b* and *c*) on the bars indicate statistically significant differences between the groups as determined by Steel-Dwass tests ($p < 0.05$). R^2, coefficient of determination; *m*, Weibull modulus; Pf, fracture probability; σ, fracture strength at a given Pf.

tion temperature (*i.e.*, 600 °C) of amorphous zirconia prepared using the sol-gel method [35] indicated that only $tZrO_2$ was formed in the coating layer and hence the mechanical properties were unchanged by annealing at 550 °C.

Another strengthening mechanism could involve direct effects on the Y-TZP substrate; *i.e.*, migration of Y ions from the Y-TZP substrate into the $mZrO_2$ coating layer during thermal annealing and/or stabilization of the monoclinic phase of Y-TZP substrate contacting the $mZrO_2$ coating layer. The migration of Y ions would de-stabilize the tetragonal phase of the Y-TZP substrate, and the compressive stress may remain on the Y-TZP substrate surface. Direct evidence for the migration of Y ions was not obtained in this study, but the increase in the thickness of monoclinic phase remained in the Y-TZP substrate support this proposed mechanism.

It should be noted that the thick coating (>0.3 μL/mm²) induced crack formation in the coating layer, and was partially removed by ultrasonic washing treatment, which may be due to the aggregation of $mZrO_2$ nanoparticles upon drying. In this study, PAA was used to disperse the $mZrO_2$ nanoparticles in ethanol through the interactions of COOH groups and zirconium ions [38]. However, PAA might be inefficient to stabilize the nanoparticle dispersion at the high nanoparticles concentration upon drying. The formation of aggregates upon drying could be prevented by optimizing the type of dispersion agent and its concentration.

In this study, sintered Y-TZP was used as a substrate for $mZrO_2$ coating. Considering the strengthening mechanism described above, the $mZrO_2$ (or amorphous zirconia) coating would also be effective to improve the mechanical properties of other types of zirconia such as highly translucent partially stabilized zirconia (PSZ) consisting of cubic zirconia ($cZrO_2$). Coating on pre-sintered zirconia followed by sintering would also be effective for improving mechanical properties, and these hypotheses will be tested in the near future.

The surface roughness increased with $mZrO_2$ coating due to the partial sintering of the nanoparticles during annealing at 1000 °C. The increased surface roughness is preferable for obtaining suitable bonding with the intended synthetic substrates, such as veneering porcelain or luting agents.

The effect of low temperature degradation (LTD) was not evaluated in this study. However, the $mZrO_2$ coating layer is expected to exhibit resistance to LTD, because LTD can be suppressed by the monoclinic phase on the zirconia surface [39] and a compressive surface stress layer is beneficial for aging resistance [40]. Thus, LTD of $mZrO_2$ coated zirconia should be investigated to confirm the long-term clinical performance of zirconia restorations.

5. Conclusions

Based on the results obtained, and within the limitations of this study, it can be concluded that the thermal annealing with the $mZrO_2$ nanoparticle coating can improve the reliability of sandblasted Y-TZP without decreasing its mechanical strength, which would otherwise be decreased by the conventional annealing process.

Acknowledgement

This work was supported in part by the Japan Society for the Promotion of Science KAKENHI Grant Numbers JP15K13303, JP18K09637 and JP18K17098.

Appendix A. Supplementary data

Supplementary material related to this article can be found, in the online version, at doi:https://doi.org/10.1016/j.dental.2019.04.002.

REFERENCES

[1] Lee K-R, Choe H-C, Heo Y-R, Lee J-J, Son M-K. Effect of different grinding burs on the physical properties of zirconia. J Adv Prosthodont 2016;8:137, http://dx.doi.org/10.4047/jap.2016.8.2.137.

[2] Pjetursson BE, Sailer I, Makarov NA, Zwahlen M, Thoma DS. All-ceramic or metal-ceramic tooth-supported fixed dental prostheses (FDPs)? A systematic review of the survival and complication rates. Part II: multiple-unit FDPs. Dent Mater 2015;31:624–39, http://dx.doi.org/10.1016/j.dental.2015.02.013.

[3] Apratim A, Eachempati P, Krishnappa Salian KK, Singh V, Chhabra S, Shah S. Zirconia in dental implantology: a review. J Int Soc Prev Community Dent 2015;5:147–56, http://dx.doi.org/10.4103/2231-0762.158014.

[4] Sailer I, Makarov NA, Thoma DS, Zwahlen M, Pjetursson BE. All-ceramic or metal-ceramic tooth-supported fixed dental prostheses (FDPs)? A systematic review of the survival and complication rates. Part I: single crowns (SCs). Dent Mater 2015;31:603–23, http://dx.doi.org/10.1016/j.dental.2015.02.011.

[5] Kelly JR, Denry I. Stabilized zirconia as a structural ceramic: an overview. Dent Mater 2008;24:289–98, http://dx.doi.org/10.1016/j.dental.2007.05.005.

[6] Thompson JY, Stoner BR, Piascik JR, Smith R. Adhesion/cementation to zirconia and other non-silicate ceramics: where are we now? Dent Mater 2011;27:71–82, http://dx.doi.org/10.1016/j.dental.2010.10.022.

[7] Tzanakakis E-GC, Tzoutzas IG, Koidis PT. Is there a potential for durable adhesion to zirconia restorations? A systematic review. J Prosthet Dent 2016;115:9–19, http://dx.doi.org/10.1016/j.prosdent.2015.09.008.

[8] Okada M, Inoue K, Irie M, Taketa H, Torii Y, Matsumoto T. Resin adhesion strengths to zirconia ceramics after primer treatment with silane coupling monomer or oligomer. Dent Mater J 2017;36:600–5, http://dx.doi.org/10.4012/dmj.2016-334.

[9] Kim HJ, Lim HP, Park YJ, Vang MS. Effect of zirconia surface treatments on the shear bond strength of veneering ceramic. J Prosthet Dent 2011;105:315–22, http://dx.doi.org/10.1016/S0022-3913(11)60060-7.

[10] Miyazaki T, Nakamura T, Matsumura H, Ban S, Kobayashi T. Current status of zirconia restoration. J Prosthodont Res 2013;57:236–61, http://dx.doi.org/10.1016/j.jpor.2013.09.001.

[11] Moon J-E, Kim S-H, Lee J-B, Han J-S, Yeo I-S, Ha S-R. Effects of airborne-particle abrasion protocol choice on the surface characteristics of monolithic zirconia materials and the shear bond strength of resin cement. Ceram Int 2016;42:1552–62, http://dx.doi.org/10.1016/j.ceramint.2015.09.104.

[12] Aurélio IL, Maria A, Marchionatti E, Montagner AF, May LG, Soares FZM. Does air particle abrasion affect the flexural strength and phase transformation of Y-TZP? A systematic review and meta-analysis. Dent Mater 2016;32:827–45, http://dx.doi.org/10.1016/j.dental.2016.03.021.

[13] Kosmac T, Oblak C, Jevnikar P, Funduk N, Marion L. Strength and reliability of surface treated Y-TZP dental ceramics. J Biomed Mater Res 2000;53:304–13, http://dx.doi.org/10.1002/1097-4636(2000)53.

[14] Luthardt RG, Holzhüter M, Sandkuhl O, Herold V, Schnapp JD, Kuhlisch E, et al. Reliability and properties of ground Y-TZP-Zirconia ceramics. J Dent Res 2002;81:487–91.

[15] Guess PC, Zhang Y, Kim JW, Rekow ED, Thompson VP. Damage and reliability of Y-TZP after cementation surface treatment. J Dent Res 2010;89:592–6, http://dx.doi.org/10.1177/0022034510363253.

[16] Hatanaka GR, Polli GS, Fais LMG, Reis JM dos SN, Pinelli LAP. Zirconia changes after grinding and regeneration firing. J Prosthet Dent 2017;118:61–8, http://dx.doi.org/10.1016/j.prosdent.2016.09.026.

[17] Ryan DPO, Fais LMG, Antonio SG, Hatanaka GR, Candido LM, Pinelli LAP. Y-TZP zirconia regeneration firing: microstructural and crystallographic changes after grinding. Dent Mater J 2017;36:447–53, http://dx.doi.org/10.4012/dmj.2016-124.

[18] Promakhov V, Kulkov N. Thermal expansion of oxide systems on the basis of ZrO_2. J Silic Based Compos Mater 2014;66:81–3.

[19] Hayashi H, Saitou T, Maruyama N, Inaba H. Thermal expansion coefficient of yttria stabilized zirconia for various yttria contents. Solid State Ion 2005;176:613–9, http://dx.doi.org/10.1016/j.ssi.2004.08.021.

[20] Ezoe M, Murase Y, Daimon K, Kato E. Formation and thermal change of monoclinic zirconia polycrystalline thin films by sol–gel process. Yogyo-Kyokaishi 1986;94:823–6.

[21] Murase Y, Kato E. Preparation of zirconia whiskers from zirconium hydroxide in sulfuric acid solutions under hydrothermal conditions at 200 °C. J Am Ceram Soc 2001;84:2705–6, http://dx.doi.org/10.1111/j.1151-2916.2001.tb01076.x.

[22] Okada M, Taketa H, Torii Y, Irie M, Matsumoto T. Optimal sandblasting conditions for conventional-type yttria-stabilized tetragonal zirconia polycrystals. Dent Mater 2019;35:169–75.

[23] Wille S, Hölken I, Haidarschin G, Adelung R, Kern M. Biaxial flexural strength of new Bis-GMA/TEGDMA based composites with different fillers for dental applications. Dent Mater 2016;32:1073–8, http://dx.doi.org/10.1016/j.dental.2016.06.009.

[24] R Development Core Team. R: a language and environment for statistical computing; 2016.

[25] Weibull W. Wide applicability. J Appl Mech 1951;103:293–7.

[26] Tiryakioğlu M, Hudak D. Guidelines for two-parameter Weibull analysis for flaw-containing materials. Metall Mater Trans B Process Metall Mater Process Sci 2011;42:1130–5, http://dx.doi.org/10.1007/s11663-011-9556-8.

[27] Hudak D, Tiryakioĝlu M. On comparing the shape parameters of two Weibull distributions. Mater Sci Eng A 2011;528:8028–30, http://dx.doi.org/10.1016/j.msea.2011.07.013.

[28] Garvie RC, Nicholson PS. Phase analysis in zirconia systems. J Am Ceram Soc 1972;55:303–5, http://dx.doi.org/10.1111/j.1151-2916.1972.tb11290.x.

[29] Toraya H, Yoshimura M, Somiya S. Calibration curve for quantitative analysis of the monoclinic-tetragonal ZrO_2 system by X-ray diffraction. J Am Ceram Soc 1984;67:C-119–21, http://dx.doi.org/10.1111/j.1151-2916.1984.tb19715.x.

[30] Kosmac T, Wagner R, Claussen N. X-ray determination of transformation depths in ceramics containing tetragonal ZrO_2. J Am Ceram Soc 1981;64:c-72–3, http://dx.doi.org/10.1111/j.1151-2916.1981.tb10285.x.

[31] Passos SP, Linke B, Major PW, Nychka JA. The effect of air-abrasion and heat treatment on the fracture behavior of Y-TZP. Dent Mater 2015;31:1011–21, http://dx.doi.org/10.1016/j.dental.2015.05.008.

[32] Kuwabara A, Tohei T, Yamamoto T, Tanaka I. Ab initio lattice dynamics and phase transformations of ZrO_2. Phys Rev B 2005;71:064301, http://dx.doi.org/10.1103/PhysRevB.71.064301.

[33] Patil RN, Subbarao EC. Axial thermal expansion of ZrO_2 and HfO_2 in the range room temperature to 1400 °C. J Appl Crystallogr 1969;2:281–8, http://dx.doi.org/10.1107/S0021889869007217.

[34] Subbarao EC, Maiti HS, Srivastava KK. Martensitic transformation in zirconia. Phys Status Solidi 1974;21:9–40, http://dx.doi.org/10.1002/pssa.2210210102.
[35] Santos V, Zeni M, Bergmann CP, Hohemberger JM. Correlation between thermal treatment and tetragonal/monoclinic nanostructured zirconia powder obtained by sol–gel process. Rev Adv Mater Sci 2008;17:62–70.
[36] Opalinska A, Malka I, Dzwolak W, Chudoba T, Presz A, Lojkowski W. Size-dependent density of zirconia nanoparticles. Beilstein J Nanotechnol 2015;6:27–35, http://dx.doi.org/10.3762/bjnano.6.4.
[37] Shahramian K, Leminen H, Meretoja V, Linderbäck P, Kangasniemi I, Lassila L, et al. Sol–gel derived bioactive coating on zirconia: effect on flexural strength and cell proliferation. J Biomed Mater Res – B Appl Biomater 2017;105:2401–7, http://dx.doi.org/10.1002/jbm.b.33780.
[38] Rothe J, Plaschke M, Denecke MA. Understanding humic acid/Zr(IV) interaction—a spectromicroscopy approach. AIP Conf Proc 2007;882:193–5, http://dx.doi.org/10.1063/1.2644471. AIP.
[39] Amaral M, Valandro LF, Bottino MA, Souza ROA. Low-temperature degradation of a Y-TZP ceramic after surface treatments. J Biomed Mater Res – B Appl Biomater 2013;101:1387–92, http://dx.doi.org/10.1002/jbm.b.32957.
[40] Deville S, Chevalier J, Gremillard L. Influence of surface finish and residual stresses on the ageing sensitivity of biomedical grade zirconia. Biomaterials 2006;27:2186–92, http://dx.doi.org/10.1016/j.biomaterials.2005.11.021.